NASA/TM—2013-217888/PART2

Low Temperature Creep of Hot-Extruded Near-Stoichiometric NiTi Shape Memory Alloy

Part II: Effect of Thermal Cycling

S.V. Raj and R.D. Noebe
Glenn Research Center, Cleveland, Ohio

June 2013

NASA STI Program . . . in Profile

Since its founding, NASA has been dedicated to the advancement of aeronautics and space science. The NASA Scientific and Technical Information (STI) program plays a key part in helping NASA maintain this important role.

The NASA STI Program operates under the auspices of the Agency Chief Information Officer. It collects, organizes, provides for archiving, and disseminates NASA's STI. The NASA STI program provides access to the NASA Aeronautics and Space Database and its public interface, the NASA Technical Reports Server, thus providing one of the largest collections of aeronautical and space science STI in the world. Results are published in both non-NASA channels and by NASA in the NASA STI Report Series, which includes the following report types:

- TECHNICAL PUBLICATION. Reports of completed research or a major significant phase of research that present the results of NASA programs and include extensive data or theoretical analysis. Includes compilations of significant scientific and technical data and information deemed to be of continuing reference value. NASA counterpart of peer-reviewed formal professional papers but has less stringent limitations on manuscript length and extent of graphic presentations.

- TECHNICAL MEMORANDUM. Scientific and technical findings that are preliminary or of specialized interest, e.g., quick release reports, working papers, and bibliographies that contain minimal annotation. Does not contain extensive analysis.

- CONTRACTOR REPORT. Scientific and technical findings by NASA-sponsored contractors and grantees.

- CONFERENCE PUBLICATION. Collected papers from scientific and technical conferences, symposia, seminars, or other meetings sponsored or cosponsored by NASA.

- SPECIAL PUBLICATION. Scientific, technical, or historical information from NASA programs, projects, and missions, often concerned with subjects having substantial public interest.

- TECHNICAL TRANSLATION. English-language translations of foreign scientific and technical material pertinent to NASA's mission.

Specialized services also include creating custom thesauri, building customized databases, organizing and publishing research results.

For more information about the NASA STI program, see the following:

- Access the NASA STI program home page at *http://www.sti.nasa.gov*

- E-mail your question to *help@sti.nasa.gov*

- Fax your question to the NASA STI Information Desk at 443–757–5803

- Phone the NASA STI Information Desk at 443–757–5802

- Write to:
  STI Information Desk
  NASA Center for AeroSpace Information
  7115 Standard Drive
  Hanover, MD 21076–1320

NASA/TM—2013-217888/PART2

Low Temperature Creep of Hot-Extruded Near-Stoichiometric NiTi Shape Memory Alloy

Part II: Effect of Thermal Cycling

S.V. Raj and R.D. Noebe
Glenn Research Center, Cleveland, Ohio

National Aeronautics and
Space Administration

Glenn Research Center
Cleveland, Ohio 44135

June 2013

Acknowledgments

This work was supported by the Subsonic Fixed Wing Project of NASA's Fundamental Aeronautics Program.

This work was sponsored by the Fundamental Aeronautics Program
at the NASA Glenn Research Center.

Level of Review: This material has been technically reviewed by technical management.

Available from

NASA Center for Aerospace Information
7115 Standard Drive
Hanover, MD 21076–1320

National Technical Information Service
5301 Shawnee Road
Alexandria, VA 22312

Available electronically at http://www.sti.nasa.gov

Low Temperature Creep of Hot-Extruded Near-Stoichiometric NiTi Shape Memory Alloy
Part II: Effect of Thermal Cycling

S.V. Raj and R.D. Noebe
National Aeronautics and Space Administration
Glenn Research Center
Cleveland, Ohio 44135

Abstract

This paper is the first report on the effect prior low temperature creep on the thermal cycling behavior of NiTi. The isothermal low temperature creep behavior of near-stoichiometric NiTi between 300 and 473 K was discussed in Part I. The effect of temperature cycling on its creep behavior is reported in the present paper (Part II). Temperature cycling tests were conducted between either 300 or 373 K and 473 K under a constant applied stress of either 250 or 350 MPa with hold times lasting at each temperature varying between 300 and 700 h. Each specimen was pre-crept either at 300 or 473 K for several months under an identical applied stress as that used in the subsequent thermal cycling tests. Irrespective of the initial pre-crept microstructures, the specimens exhibited a considerable increase in strain with each thermal cycle so that the total strain continued to build-up to 15 to 20 percent after only 5 cycles. Creep strains were immeasurably small during the hold periods. It is demonstrated that the strains in the austenite and martensite are linearly correlated. Interestingly, the differential irrecoverable strain, $\Delta\varepsilon_{irr}$, in the material measured in either phase decreases with increasing number of cycles, N, as $\Delta\varepsilon_{irr} = 4.3(N)^{-0.5}$ similar to the well-known Manson-Coffin relation in low cycle fatigue. Both phases are shown to undergo strain hardening due to the development of residual stresses. Plots of true creep rate against absolute temperature showed distinct peaks and valleys during the cool-down and heat-up portions of the thermal cycles, respectively. Transformation temperatures determined from the creep data revealed that the austenitic start and finish temperatures were more sensitive to the pre-crept martensitic phase than to the pre-crept austenitic phase. The results are discussed in terms of a phenomenological model, where it is suggested that thermal cycling between the austenitic and martensitic phase temperatures or vice versa results in the deformation of the austenite and a corresponding development of a back stress due to a significant increase in the dislocation density during thermal cycling.

1.0 Introduction

As noted in Part I (Ref. 1), NiTi shape memory alloys (SMA) are being considered for use as solid state actuators (Ref. 2). By design, the SMA actuators would be required to undergo thermal cycles under constant or variable loading conditions. However, thermal cycling tests on most SMAs under an applied stress result in irrecoverable strain at the end of each cycle so that the start and end points do not coincide thereby reducing the useful life of actuators in actual applications (Ref. 3). The occurrence of these irrecoverable strains has been attributed to transformation-induced plasticity (Refs. 4, 5, 6, 7, 8, 9, 10, and 11). These constant load thermal cycling tests have been conducted primarily using a servo-hydraulic machine so that long term creep effects have not been evaluated. In particular, the effect of prior long duration isothermal creep deformation lasting several months on subsequent constant load thermal cycling tests have not been investigated to date. Earlier constant load or constant stress creep studies on NiTi were conducted above 743 K corresponding to the austenitic phase field (Refs. 12, 13, 14, 15, 16, 17, and 18) and well above the application temperature range for NiTi actuators. Consequently, the long term isothermal creep behavior of NiTi between room temperature and 473 K under constant applied stresses varying between 200 and 350 MPa was investigated as part of this investigation and the results are reported in Part I (Ref. 1). Based on earlier studies on the deformation behavior of NiTi (Refs. 2, 3, 4,

11, 19, 20, 21, 22, 23, 24, 25, and 26), the predominant creep microstructures in the specimens studied in Pt. I (Ref. 1) are expected to be primarily detwinned martensite (M) and "dislocated" austenite (A) consisting of a mixture of dislocations and deformation twins necessary to satisfy von Mises criterion (Ref. 27). Recent short-term constant load creep tests conducted on a Ti-rich NiTi at 773 K confirm the formation of an extensive dislocation and deformation twinned microstructure (Ref. 18).

The objectives of the present paper are to report the effects of temperature cycling on the creep behavior of pre-crept NiTi under constant load conditions. Unlike previous investigations (Refs. 3, 4, 5, 6, 7, 8, 9, and 10), where the specimens that were thermally cycled generally had an undeformed microstructure prior to testing, the specimens used in this investigation were first isothermally crept under constant load conditions for several thousand hours prior to thermally cycling them.

2.0 Experimental Procedures

Details of the alloy composition and testing procedures are described in Part I (Ref. 1). A total of three specimens were thermally cycled. The first two specimens were isothermally pre-crept either at 300 K for 5205.7 h to a true creep strain, ε, of about 4.3 percent ((a) (Ref. 1)) or at 473 K for 4342.1 h to $\varepsilon \approx 1.1$ percent (Fig. 8(b) (Ref. 1)) under an applied stress,σ, of 350 MPa. As stated earlier, the expected creep microstructures at these values of ε are detwinned martensite and "dislocated" austenite at 300 and 473 K, respectively. Subsequently, both specimens were thermally cycled between 300 and 473 K under an applied stress of 350 MPa. A third specimen was pre-crept at 473 K for about 5062 h to $\varepsilon \approx 1.6$ percent under an initial applied stress of 250 MPa (Fig. 8(a) (Ref. 1)) prior to thermally cycling between 373 and 473 K while maintaining the applied stress. In all three cases, the specimen was held at each new temperature for 300 to 700 h before changing to the previous temperature in order to distinguish between the strain contributions from isothermal creep during the hold time from those due to thermal cycling.

3.0 Results

3.1 Thermal Cycling Creep Curves

Figure 1 shows the variations in the true creep strain and absolute temperature, T, with increasing creep time, t, as T varied between $T_1 = 473$ K and $T_2 = 373$ K, where T_1 and T_2 are the initial and final temperatures, respectively, for a specimen crept under an initial applied stress of 250 MPa for 5061.6 h (Fig. 8(a) in (Ref. 1)). Only the thermal cycling portions of the ε - t curve are shown in the figure for better clarity. The specimen was held at each temperature for varying hold times between 312 and 650 h. The two broken curves show the increase in total strain at either 373 or 473 K. An examination of Figure 1 reveals that the total strain at the end of each cycle was higher than at the start of the cycle so that the strain in the material continued to ratchet up with each additional thermal cycle. Thus, the total strain increased from about 1.6 percent at the commencement of the first thermal cycle to about 5.4 percent at the end of the fifth thermal cycle; a maximum strain of 8.7 percent was observed after the fifth temperature decrease from 473 to 373 K. For comparison, the measured isothermal creep strain at 473 K increased from 1.1 percent on loading to 1.5 percent after 2709 h under an initial creep stress of 250 MPa (Refs. 1). This corresponds to an approximate creep rate of about 4×10^{-10} s^{-1}, so that the relatively short duration hold times at each temperature are unlikely to significantly influence the measured strain in these thermal cycling tests. Thus, the observed thermal ratcheting can be attributed almost entirely to temperature cycling effects under the present loading conditions.

Figure 2(a) shows the ε-t plot for variations of T between $T_1 = 300$ and $T_2 = 473$ K for the specimen pre-crept at 300 h for several months under an initial creep stress of 350 MPa to a $\varepsilon \approx 4.3$ percent prior to the thermal cycling tests at the same stress (i.e., "detwinned" martensite); the same data are replotted as a ε-T plot for ease of comparison with data obtained from stress-strain curves (Refs. 2, 3, and 8) (Figure 2(b)). At the start of the first cycle, ε decreased from 4.3 to 2.3 percent as the absolute temperature

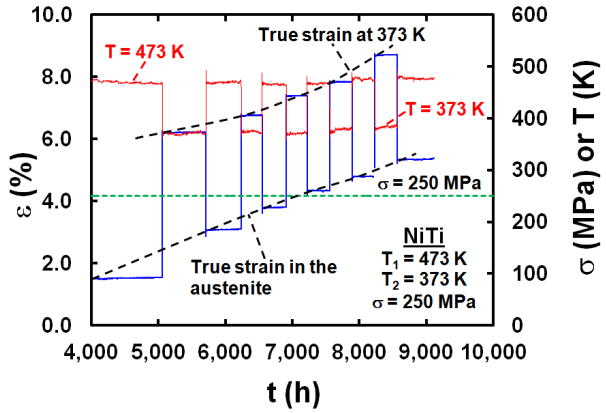

Figure 1.—Variation of the true creep strain and absolute temperature with creep time for a specimen pre-crept for 5061.6 h at 473 K and then thermally cycled between 473 and 373 K under an applied stress of 250 MPa.

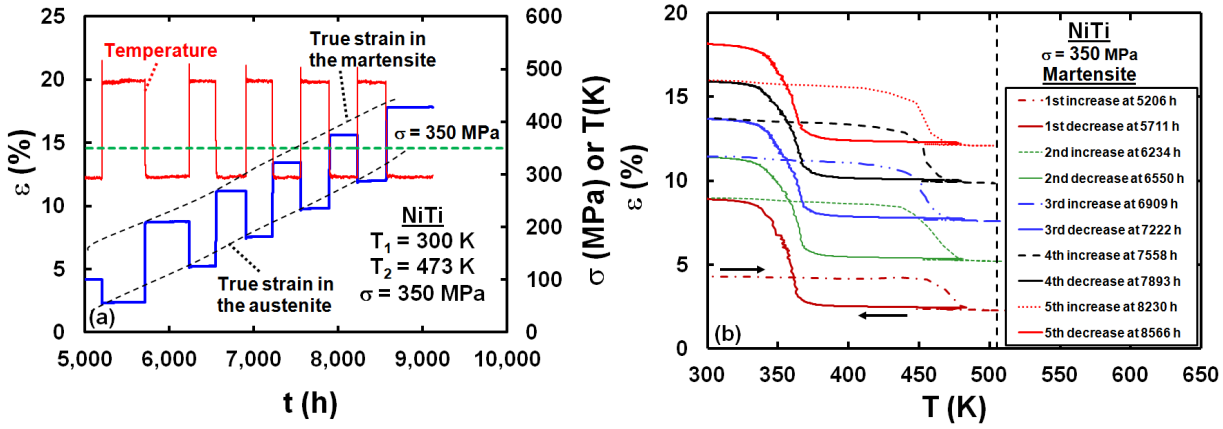

Figure 2.—(a) True creep strain versus creep time and (b) true creep strain versus absolute temperature for a specimen pre-crept at 300 K under an applied stress of 350 MPa and subsequently thermally cycled between 300 and 473 K.

increased from 300 to 473 K as the martensite transformed to austenite so that the decrease in the amount of creep strain was 2.0 percent. The specimen was held for about 505 h at 473 K prior to decreasing the temperature to 300 K, where the measured creep strain was 0.08 percent corresponding to an approximate creep rate of about 4.4×10^{-10} s^{-1}. For comparison, the estimated isothermal creep rates at 300 K prior to thermal cycling were of the order of 1.5×10^{-10} s^{-1}. The variation in strain was insignificant during this hold period. On decreasing the temperature from 473 K to room temperature, the magnitude of ε increased to 8.7 percent as the austenite transformed to martensite. Significantly, the increase in the amount of true strain by 4.4 percent at the end of the cycle was much greater than the strain of 4.3 percent at the beginning of the cycle thereby signifying a large irrecoverable strain residual in the specimen after the first thermal cycle. As noted above, this plastic strain is predominantly due to thermal ratcheting rather than creep under these conditions. Continued thermal cycling of the specimen resulted in a large strain build-up in the specimen so that $\varepsilon \approx 17.8$ percent after N = 5 cycles, where N is the number of thermal cycles. The total strain in the austenite and the martensite continued to increase almost linearly as shown by the two broken lines in Figure 2(a).

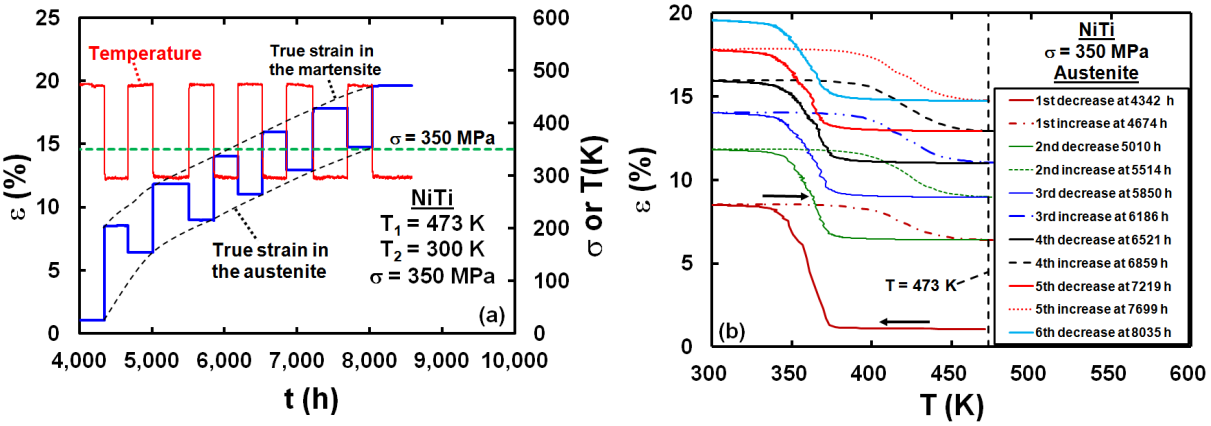

Figure 3.—(a) True creep strain versus creep time and (b) true creep strain versus absolute temperature for a specimen pre-crept at 473 K under an applied stress of 350 MPa and subsequently thermally cycled between 473 and 300 K.

Similarly, decreasing the temperature from T_1 = 473 K to T_2 = 300 K as in the case of the specimen pre-crept at 473 K resulted in an increase in ε from about 1.1 to 8.5 percent as the austenite transforms to martensite (Figure 3(a)); the corresponding ε-T plot is shown in Figure 3(b). The specimen was isothermally crept at 300 K for about 321 h at 300 K before increasing the temperature back to 473 K. The estimated creep rate during this hold time at 300 K was about 1.8×10^{-10} s^{-1} with a total strain accumulation of about 0.02 percent. For comparison, the isothermal creep rates at 473 K prior to thermal cycling were estimated to be about 1.2×10^{-10} s^{-1}. A subsequent increase from 300 to 473 K resulted in a corresponding decrease in ε to 6.4 percent. The total true irrecoverable strain residual in the specimen at the end of the first thermal cycle was 5.3 percent. Once again, the total strain in the austenite and martensite continued to increase with each thermal cycle as indicated by the broken lines. At the end of N = 6 cycles, the creep strain measured in the martensitic phase was 19.6 percent.

3.2 Effect of Thermal Cycling on Deformation and Transformation Strains

Several terms are defined in this paper using Figure 4(a) and (b), which are reproduced portions of the T–t and ε-t responses for the two thermally cycled specimens under an applied stress of 350 MPa (Figure 2(a) and Figure 3(a)). The isothermal creep strains, ε_{creep}, are represented by the broken lines. The range of each cycle, N, is also shown in the figures. It should be noted that Figure 4(a) and (b) are out-of-phase by half a cycle. First, ε_{NA} and ε_{NM} are the average creep strains in the austenitic and martensitic phases, respectively,[1] accumulated at the N^{th} thermal cycle and they are measured with respect to ε = 0, i.e., ε_{NA} and ε_{NM} are absolute values of strain. They represent the average strain in the two phases at the N^{th} cycle due to thermal cycling between the two temperatures since the strain contributions during the hold periods were insignificant. Second, $(\varepsilon_{tr})_{NA}$ and $(\varepsilon_{tr})_{NM}$ are the transformation strains associated with either martensite to austenite or austenite to martensite transformations, respectively, in the N^{th} thermal cycle. Third, $(\Delta\varepsilon_{irr})_{NA}$ and $(\Delta\varepsilon_{irr})_{NM}$ are the differential irrecoverable austenitic and martensitic strains, respectively, in the N^{th} thermal cycle. Fourth, $\Delta\varepsilon_A$ and $\Delta\varepsilon_M$ are the differential true strains with respect to the isothermal creep strain lines. In other words, they represent the cumulative strains due to thermal cycling.

[1] It is noted that ε_I (I = A or M), $(\varepsilon_{tr})_I$, and $(\Delta\varepsilon_{irr})_I$ are identified with the major constituent, either austenite or martensite, in this paper for simplicity. This assumption is a reasonable first order approximation although it is noted that thermally cycling a specimen from one temperature to another could stabilize one or the other phase as a minor constituent in the microstructure to some extent.

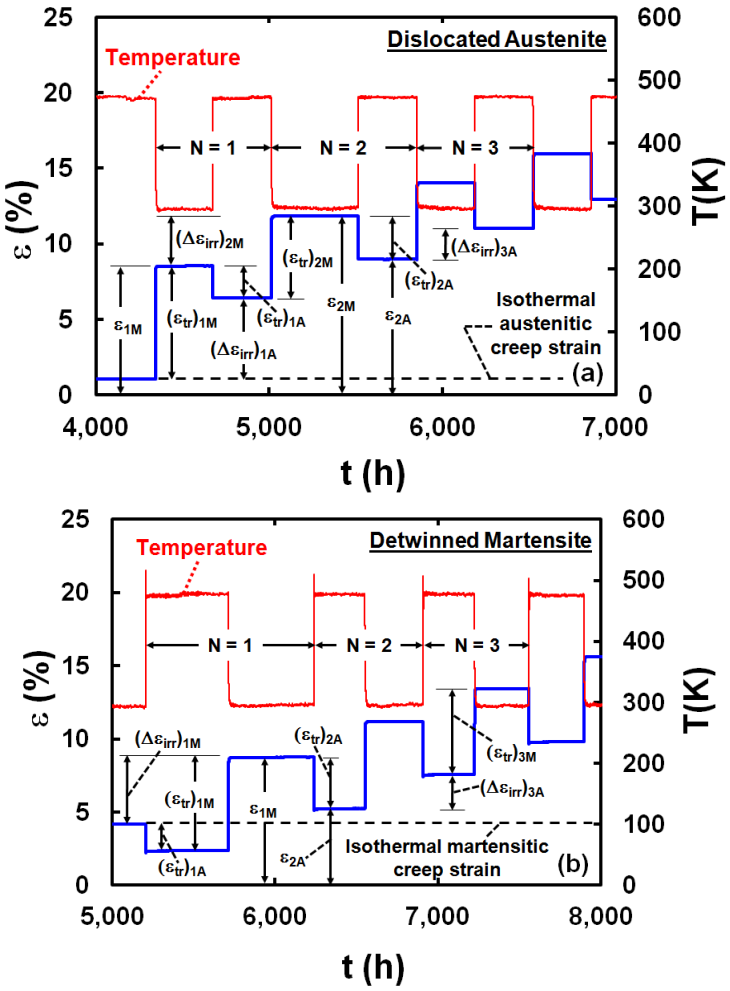

Figure 4.—Schematic of the strain- time plot for thermal cycles from (a) 473 to 300 K and (b) 300 to 473 K illustrating the various terminologies used in this paper. The broken horizontal line refers to the isothermal creep strain prior to thermal cycling. The suffixes refer to the strain in the phase (austenite (A) or martensite (M)) for the N^{th} cycle.

An examination of Figure 4(a) for the "dislocated" pre-crept austenitic microstructure gives the following algebraic relationships for N = 1, 2, 3…N:

$$(\varepsilon_{tr})_{NA} = \varepsilon_{NM} - \varepsilon_{NA} \tag{1a}$$

$$(\varepsilon_{tr})_{NM} = \varepsilon_{NM} - \varepsilon_{(N-1)A} \tag{1b}$$

$$(\Delta\varepsilon_{irr})_{NA} = \varepsilon_{NA} - \varepsilon_{(N-1)A} \tag{1c}$$

$$(\Delta\varepsilon_{irr})_{NM} = \varepsilon_{NM} - \varepsilon_{(N-1)M} \tag{1d}$$

Similarly, for the "detwinned" pre-crept martensite corresponding to Figure 4(b), the relationships for N = 1, 2, 3 ….N are:

$$(\varepsilon_{tr})_{NA} = \varepsilon_{(N-1)M} - \varepsilon_{NA} \tag{2a}$$

$$(\varepsilon_{tr})_{NM} = \varepsilon_{NM} - \varepsilon_{NA} \tag{2b}$$

$$(\Delta\varepsilon_{irr})_{NA} = \varepsilon_{NA} - \varepsilon_{(N-1)A} \tag{2c}$$

$$(\Delta\varepsilon_{irr})_{NM} = \varepsilon_{NM} - \varepsilon_{(N-1)M} \tag{2d}$$

The differential strain, $\Delta\varepsilon_A$ and $\Delta\varepsilon_M$, are defined with respect to the isothermal creep line (Figure 4(a) and (b)) as follows:

$$\Delta\varepsilon_A = \varepsilon_{NA} - \varepsilon_{creep} \tag{3a}$$

$$\Delta\varepsilon_M = \varepsilon_{NM} - \varepsilon_{creep} \tag{3b}$$

Figure 5 shows the variation of the differential strains, $\Delta\varepsilon_A$ and $\Delta\varepsilon_M$ with increasing N for the two specimens thermally cycled between 300 and 473 K under an initial applied stress of 350 MPa. Several observations can be made from Figure 5. First, the curves show a non-linear behavior so that the magnitudes of $\Delta\varepsilon_A$ and $\Delta\varepsilon_M$ decrease with increasing N thereby suggesting that both phases undergo strain hardening as the specimens are thermally cycled between the two temperatures due to the development of a back stress in the material. Second, the magnitudes of $\Delta\varepsilon_A$ and $\Delta\varepsilon_M$ for the "dislocated" and detwinned creep microstructures are nearly identical. This result is attributed to a fortuitous coincidence and no special significance is inferred from the observation. Third, the differences between $\Delta\varepsilon_A$ and $\Delta\varepsilon_M$ observed in Figure 5 represent the transformation strains. Thus, $(\varepsilon_{tr})_{NA} = \Delta\varepsilon_{NM} - \Delta\varepsilon_{NA}$ and $(\varepsilon_{tr})_{NM} = \Delta\varepsilon_{NM} - \Delta\varepsilon_{(N-1)A}$ for the "dislocated" austenite (Figure 4(a)), and $\Delta(\varepsilon_{tr})_{NA} = \Delta\varepsilon_{(N-1)M} - \Delta\varepsilon_{NA}$ and $(\varepsilon_{tr})_{NM} = \Delta\varepsilon_{NM} - \Delta\varepsilon_{NA}$ for the "detwinned" martensite (Figure 4(b)), respectively.

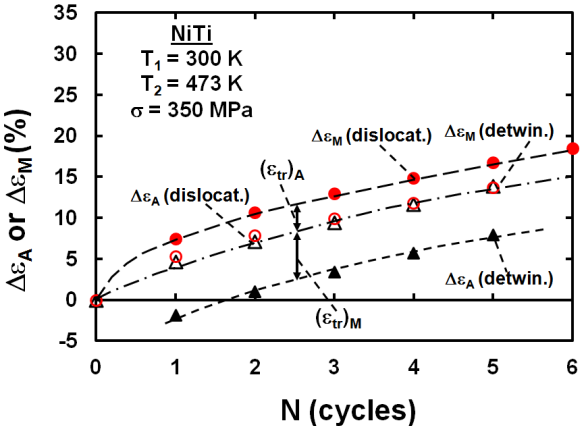

Figure 5.—Variation of the differential strains in the austenite and martensite with the number of thermal cycles for specimens initially pre-crept at 300 K (circles) and 473 K (triangles) under an applied stress of 350 MPa.

Interestingly, ε_A and ε_M exhibit a linear correlation during thermal cycling under an initial applied stress of 350 MPa for pre-crept specimens except that both sets of data are laterally displaced with respect to each other (Figure 6). This lateral displacement can be attributed to the fact that the initial strain in the specimen pre-crept at 473 K was much higher than that in the specimen pre-crept at 300 K. The slopes of the regression lines are close to unity thereby suggesting that the strain in the austenitic phase in one-half cycle is in close correspondence with that in the martensitic phase in the other half cycle irrespective of whether the specimen was pre-crept at 300 or 473 K prior to the thermal cycling tests. However, the fact that the slopes of both plots are close to unity suggests that the strain evolution in both specimens is similar irrespective of the pre-crept conditions. Especially notable are the magnitudes of ε_A and ε_M, which are surprisingly large. It was postulated in Part I (Ref. 1) that the B2 austenitic phase with three independent slip systems exhibits significant creep due to a combination of dislocation glide and deformation twinning, which satisfy von Mises criterion (Ref. 27). A similar mechanism can account for the large values of ε_A observed in Figure 6 as the austenitic phase deforms during thermal cycling. Alternatively, the activation of several slip systems provides a rationale for these large strains (Ref. 11). This rationale would suggest that the deformation microstructure in the austenite influences the magnitude of ε_M both by influencing the nucleation of the martensitic plates as well as stabilizing the martensite, as the specimen is thermally cycled between 300 and 473 K.

Figure 7 shows the variations of $(\varepsilon_{tr})_A$ and $(\varepsilon_{tr})_M$ with increasing values of N for the specimens pre-crept at 300 and 473 K. The effect of the initial creep microstructures on $(\varepsilon_{tr})_A$ and $(\varepsilon_{tr})_M$ are minimal so that the broken curves represent a reasonable approximation of the observed trend. The magnitudes of $(\varepsilon_{tr})_A$ and $(\varepsilon_{tr})_M$ decrease and increase, respectively, with increasing values of N until N = 3 after which both transformation strains approach a degree of constancy. In this case, $(\varepsilon_{tr})_M$ decreases from a maximum value of about 7.5 percent at N =1 to a minimum value of about 4.8 percent at N = 6, while $(\varepsilon_{tr})_A$ increases from a minimum value of about 1.9 percent at N =1 to a maximum value of about 3.7 percent at N = 5. Correspondingly, the ratio $(\varepsilon_{tr})_M/(\varepsilon_{tr})_A$ decreases from about 3.5 at N = 1 to about 1.6 at N = 5 irrespective of the initial pre-crept microstructure. The fact that the austenite and the martensite undergo strain hardening due to the development of an effective back stress (Figure 5) and the transformation strains evolve to approximately constant values during thermal cycling indicates that the relative volume fractions of the austenite and the martensite are also influenced by the evolution of this back stress with continued thermal cycling.

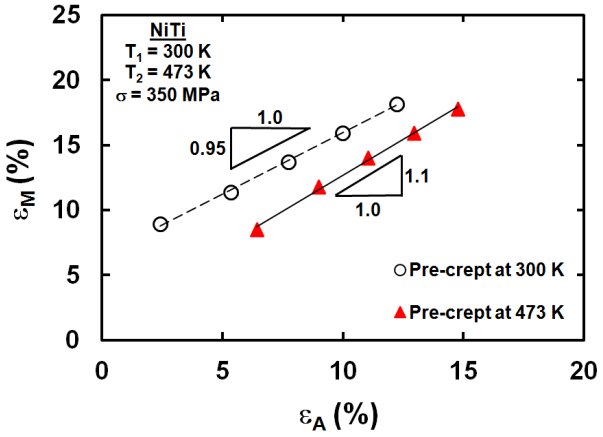

Figure 6.—Correlation between the cumulative strains in the austenitic and martensitic phases during thermal cycling in specimens pre-crept at 300 K (open circles) and 473 K (solid triangles) under an applied stress of 350 MPa.

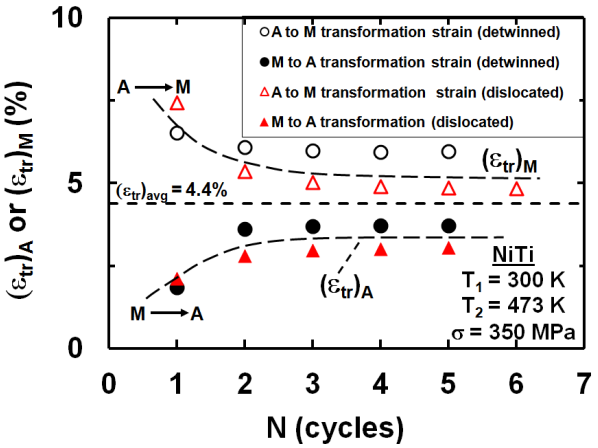

Figure 7.—Variation of the transformation strains with increasing number of thermal cycles as the austenite transforms to martensite and vice versa during thermal cycling under an applied stress of 350 MPa. The data for the specimens pre-crept at 300 and 473 K are represented by circles and triangles, respectively.

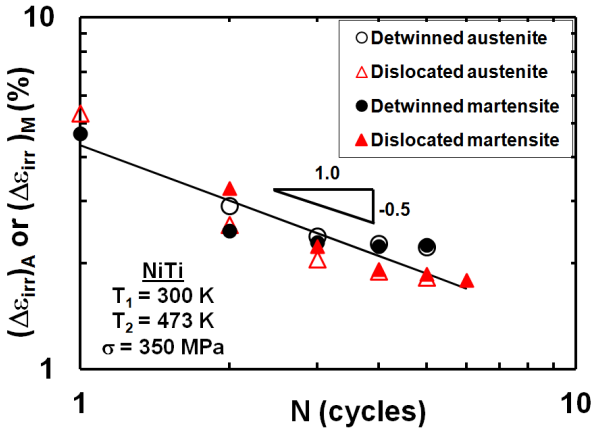

Figure 8.—Double logarithmic plot of the differential irreversible strains in the austenite and martensite against number of thermal cycles for specimens pre-crept at 300 K (circles) and 473 K (triangles).

3.3 Effect of Pre-Crept Microstructures on Differential Irrecoverable Strains

Figure 8 shows a double logarithmic plot of $(\Delta\varepsilon_{irr})_A$ and $(\Delta\varepsilon_{irr})_M$ against N for the two specimens isothermally pre-crept under an applied stress of 350 MPa. Two important points may be noted from the figure. First, both $(\Delta\varepsilon_{irr})_A$ and $(\Delta\varepsilon_{irr})_M$ decrease linearly with increasing N with the data scattered uniformly about a single regression line drawn through all the data irrespective of whether the measurements of $\Delta\varepsilon_{irr}$ were determined for the austenite or martensite. Second, the data are well represented by the regression equation:

$$\Delta\varepsilon_{irr} = (\Delta\varepsilon_{irr})_A = (\Delta\varepsilon_{irr})_M = 4.3\ N^{-0.5}\ (R_d^2 = 0.838\ ) \quad (4)$$

where R_d^2 is the coefficient of determination. The data are clustered along this regression line independent of the pre-crept microstructure. Significantly, Equation (4) is remarkably similar to the Manson-Coffin relation in low cycle fatigue (Ref. 27). Interestingly, the Manson-Coffin relation was observed during the low cycle mechanical fatigue of NiTi at room temperature, where the value of the exponent was reported to be about 0.2 (Ref. 28). Once again, Figure 8 suggests that the back stress increases in the material with increasing number of thermal cycles.

3.4 Creep Rate-Temperature Plots

Figure 9(a) to (d) show the variation of the creep rates, $\dot{\varepsilon}$, with T for the specimens pre-crept at 300 and 473 K during either the austenite to martensite forward transformation (Figure 9(a) and (b)) or the martensite to austenite reverse transformation (Figure 9(c) and (d)) of the thermal cycles, where the $\dot{\varepsilon}$ values were evaluated by differentiating the ε–t curves shown in Figure 2(a) and Figure 3(a). The cool down curves for each half cycle during the forward transformation are superimposed on the same plot in Figure 9(a) and (b), whereas the corresponding heat-up curves during the reverse transformation are superimposed in Figure 9(c) and (d). Noting that the product $\sigma\dot{\varepsilon}$ has units of power density, Figure 9 9(a) and (b) represent energy emission as the austenite transforms to martensite for the forward transformation while Figure 9(c) and (d) represent the energy absorption as the martensite transforms to austenite for the reverse transformation.

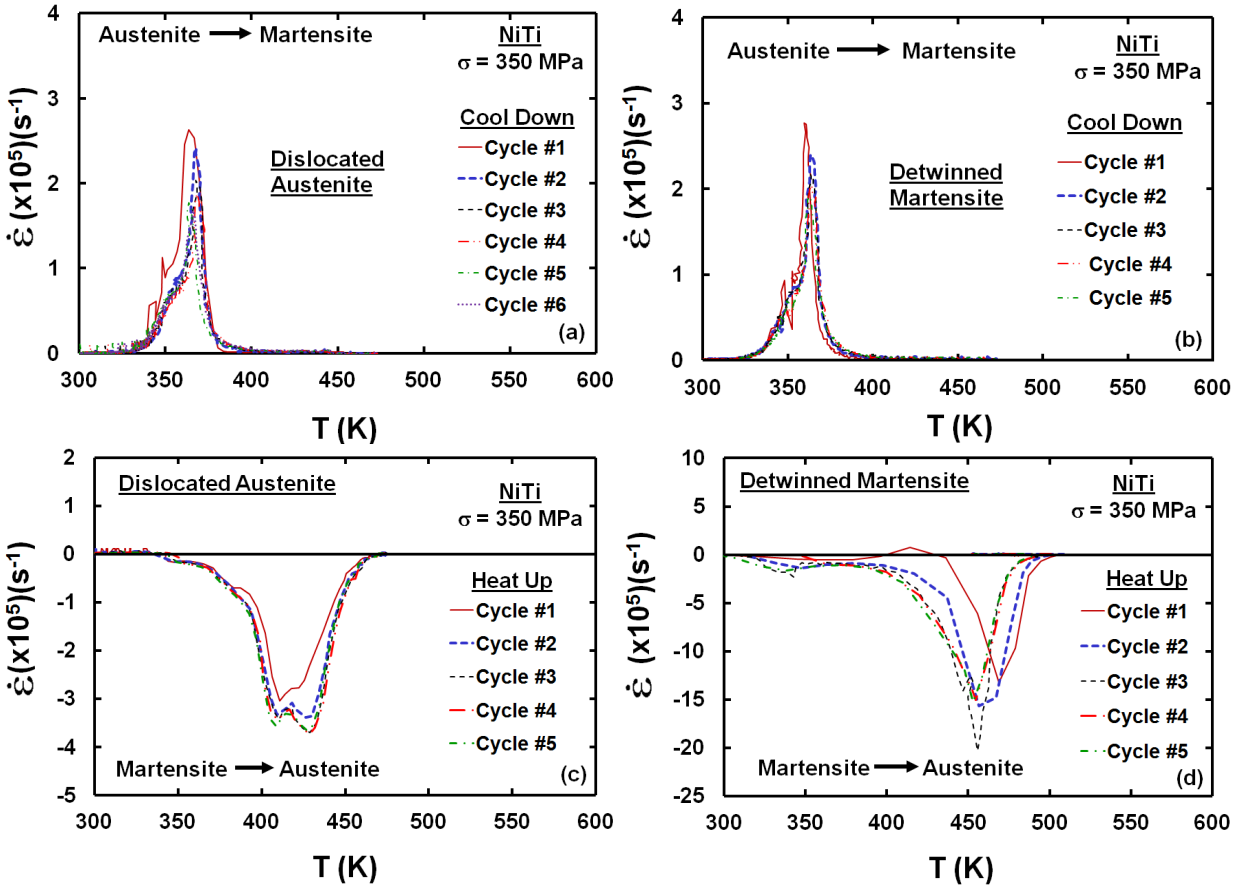

Figure 9.—True creep rate versus absolute temperature for specimens; (a) and (c) pre-crept at 300 K; (b) and (d) pre-crept at 473 K; (a) and (b) forward transformation; and (c) and (d) reverse transformation.

A close examination of Figure 9(a) and (b) reveals that all the curves superimpose for the forward transformation irrespective of the pre-crept microstructures. Similarly, the curves nearly superimpose for the specimen pre-crept at 473 K for the reverse transformation (Figure 9(c)). In contrast, the $\dot{\varepsilon}$–T curves for the specimen pre-crept at 300 K exhibited a somewhat more complex behavior for the reverse transformation (Figure 9(d)). In this case, the $\dot{\varepsilon}$–T curves shifted to lower temperatures after the first and second thermal cycles before superimposing on each other from the third cycle onwards. Additionally, the slopes of the $\dot{\varepsilon}$–T curves, as indicated by the magnitudes of $\dot{\varepsilon}$, were steeper than the results shown in Figure 9(c). In other words, the kinetics of the martensite to austenite transformation occurs at a faster rate for the specimen pre-crept at 300 K (Figure 9(d)) than for that pre-crept at 473 K (Figure 9(c)). The precise reason for this difference in behavior between the two specimens during reverse transformation is unclear.

A close examination of Figure 9(d) reveals that the tails of the transformation curves are increasingly skewed towards the lower temperatures with increasing number of thermal cycles. The curves are less skewed for the specimen pre-crept at 473 K (Figure 9(c)). These observations suggest that the reverse martensite to austenitic transformation commences at lower and lower temperatures with each thermal cycle presumably due to the build-up of the effective back stresses in the material.

The absolute transformation temperatures, T_{tr}, where T_{tr} represents the austenitic start, A_s, austenitic finish, A_f, martensitic start, M_s, and martensitic finish, M_f, temperatures, were determined from the ε-T curves (Figure 2(b) and Figure 3(b)). The rise and fall segments of these curves were extremely non-linear, and therefore it was felt that T_{tr} determined by the intercept method (Ref. 8) was unreliable. Thus, the data were determined by the deviation method, where the magnitudes of T_{tr} were identified with the points at which the curves deviated from the extensions of the stable regions (Figure 10).

Figure 11 shows the variation of T_{tr} with N for the two specimens with different pre-crept microstructures. Several points may be noted from Figure 11. First, M_s and M_f are independent of the initial creep microstructure. Second, M_s increases slightly while M_f does not vary significantly with increasing N irrespective of the pre-crept microstructures. Third, the values of A_s decrease with increasing N and they are sensitive to the pre-crept microstructure such that the values of A_s are significantly larger for the specimen pre-crept at 300 K than that pre-crept at 473 K. In the latter case, the A_s for the specimen with an expected microstructure of dislocations and deformation twins is similar to the values of M_s after N = 3. Fourth, A_f for the specimen pre-crept at 300 K decreases with increasing N and it is larger than that for the specimen pre-crept at 473 K for which A_f is independent of N. Fifth, the transformation of the martensite to austenite during the reverse transformation cycle occurs over a larger temperature range for the specimen pre-crept at 473 K than for the one pre-crept at 300 K.

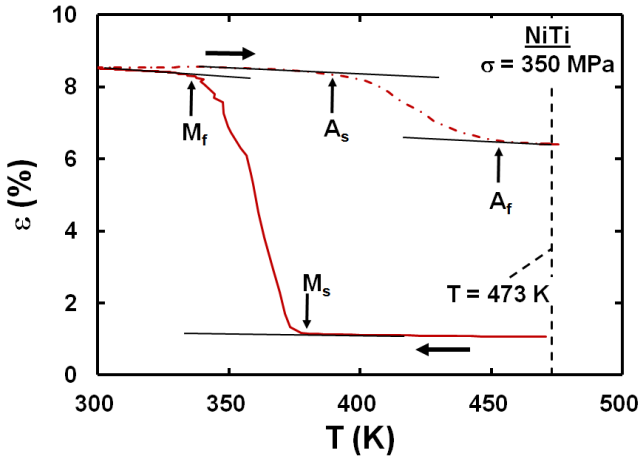

Figure 10.—Illustration of the deviation method used to determine the transformation temperatures, A_s, A_f, M_s and M_f.

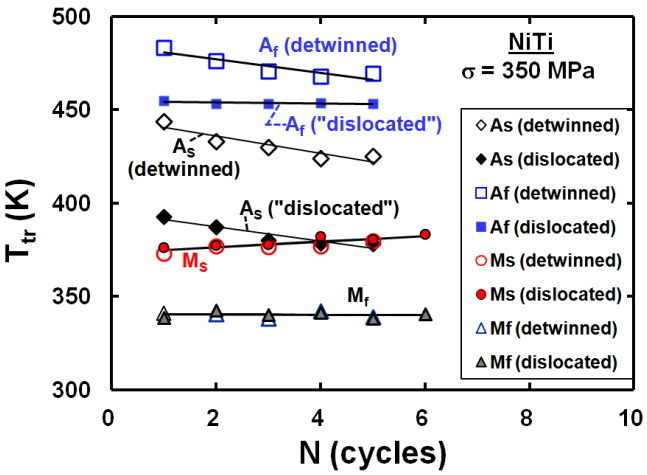

Figure 11.—Effect of pre-crept microstructures on the variations of the transformation temperatures with the number of thermal cycles.

4.0 Discussion

The observations reported in this paper have an important bearing on the design and applications of binary NiTi actuators. As shown in Figure 1 to Figure 3, thermally cycling NiTi between either 300 or 373 and 473 K under an applied stress of either 250 or 350 MPa results in a ratcheting of the total strain with each cycle. The accumulated strains are extremely large and well above 15 percent after five thermal cycles. However, the effect of hold times varying between 300 and 700 h did not significantly contribute to the total accumulated strain presumably because the creep rates were very low varying between about 2 and 5×10^{-10} s^{-1}. Based on the isothermal creep results reported in Part I (Ref. 1), where the creep strain was significant after several months, it is anticipated that long hold times lasting several months and years, would contribute to some extent, although much less than the transformation strain, to the total accumulated strain during the thermal cycling tests. Although the effect of hold time on the total strain accumulated during thermal cycling tests must be evaluated more completely than reported in the present paper, it is reasonable to suggest that hold times effects are likely to be subtle due to the evolution of the deformation microstructures. As noted in Part I (Ref. 1), measurable primary creep was observed between 300 and 473 K for stresses above 200 MPa although the creep of the austenitic phase was significantly higher than that of the martensitic phase. Thus, the effects of long hold times at 473 K lasting several months between each thermal cycle under a constant applied load are expected to be more significant than similar hold times at 300 K.

In attempting to design SMA actuators, it is essential to understand the fundamentals of the creep behavior of the austenitic and martensitic phases. It was concluded in Part I (Ref. 1) that the creep of NiTi at 300 K results in the detwinning of the martensitic twin variants on loading followed by dislocation glide-controlled primary creep. However, it was hypothesized that primary creep of NiTi at 473 K resulting in significant strain accumulation is due to the development of dislocation and deformation twin microstructures in the austenitic phase. The formation of deformation twins is necessary to accommodate the limited slip systems in its B2 crystal structure.

The effects of these two pre-crept microstructures on the subsequent thermal cycling behavior of NiTi reported in this paper can be summarized as follows: (a) The material undergoes strain hardening with increasing number of thermal cycles thereby indicating a build-up in residual stress (Figure 5). This increase in residual stress can be attributed to the development of dislocation microstructures during each thermal cycle. (b) Significantly, the creep strains in the austenitic and the martensitic phases are closely correlated so that the strain in one phase increases as the strain in the other phase increases (Figure 6).

Thus, the deformation microstructures formed in the austenite at 473K are not destroyed after it transforms to martensite when the specimen is cooled to 300 K. Instead, it appears that the deformation of one phase in the first half of the thermal cycle influences the deformation of the other phase in the second half of the thermal cycle irrespective of the initial creep microstructure. (c) The observed inverse linear correlation between $\Delta\varepsilon_{irr}$ and N shown in Figure 8, and described by Equation (2) similar to the Manson-Coffin relation in low cycle fatigue (Ref. 27), is also consistent with the formation of a dislocation substructure and the development of an associated back stress.

The observed variations in T_{tr} with increasing N shown in Figure 11 suggest that the A_s and A_f temperatures are acutely sensitive to the initial isothermal creep microstructure prior to thermal cycling unlike M_s and M_f. The deformation microstructures developed during isothermal creep of the austenitic phase at 473 K reduces the magnitudes of the A_s and A_f transformation temperatures well below those for the specimen isothermally pre-crept at 300 K in the martensitic phase field. The decrease in A_f with increasing N for both pre-crept microstructures suggests that it becomes progressively easier to complete the reverse martensite-to-austenite transformation with each thermal cycle. The present observed trends in the transformation temperatures during thermo-mechanical cycling are not always consistent with earlier observations on the thermal cycling behavior of NiTi. For example, Grossman et al. (Ref. 29) reported that M_s and M_f increase, while A_s and A_f were essentially constant, with increasing N during constant load thermomechanical cycling of a near-equiatomic binary NiTi.

The observations shown in Figure 11 can be rationalized in terms of the time evolution of the ε–T plots (Figure 12). Prior to the commencement of the thermal cycling experiments corresponding to N = 0, the hysteresis of the ε-T plots is relatively large so that A_s is much greater than M_s as indicated by the two vertical broken lines in Figure 12. With continued thermal cycling, the A_s and A_f decrease significantly while M_s increases slightly with increasing N for the specimen pre-crept at 300 K (Figure 11), thereby indicating a reduction in the width of the hysteresis with each thermal cycle as the reverse transformation curve moves to lower temperatures in Figure 12. The small increase in M_s to higher temperatures while M_f remains unchanged indicates that the slope of the forward transformation (i.e., austenite to martensite) curve

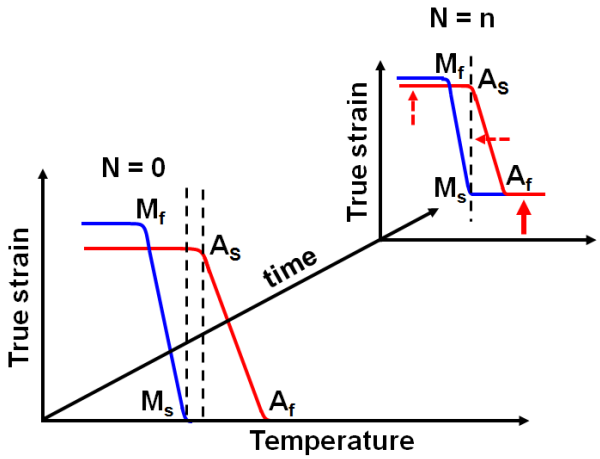

Figure 12.—Schematic showing the relative shifts in the positions of the transformation temperatures during thermal cycling with respect to the true strain versus absolute temperature plot.

decreases in the ε-T plot with increasing N. The decrease in the A_s and a slight increase in the M_s with increasing N for the specimen pre-crept at 473 K also indicates a reduction in the hysteresis but since A_f is independent of N, the slope of the reverse transformation curve in the ε-T plot decreases with increasing N. The close correspondence between ε_A and ε_M (Figure 6) and the increase in $\Delta\varepsilon_A$ and $\Delta\varepsilon_M$ with increasing N (Figure 5) suggests that the ε-T plot moves upwards parallel to the creep strain axis in Figure 12.

The slopes of the forward transformation curves observed in the ε–T plots are influenced by the stored elastic strain energy due to the formation of the martensite, whereas the slopes of the reverse transformation are influenced by the dissipation of this stored elastic energy (Refs. 30, 31, and 32). Thus, a large difference between the M_s and M_f transformation temperatures corresponds to a shallow slope and leads to a high stored elastic strain energy, whereas a small difference between these two transformation temperatures corresponds to a steeper slope and lower stored elastic energy.

Similarly, the width of the hysteresis is indicative of the frictional resistance to the motion of the austenite-martensite interfaces and martensite-martensite interfaces with different crystallographic orientations (Refs. 30, 31, and 32). A narrow hysteresis suggests a decreased frictional resistance to interfacial motion and a low relaxation of the stored elastic energy during the martensite to austenite reverse transformation. However, a wide hysteresis indicates a large frictional resistance and a high relaxation of the stored elastic energy. The A_s and A_f temperatures are expected to be lower for a ε-T plot with a narrow hysteresis than for one with a wider hysteresis. Thus, the observed decrease in A_s and A_f with increasing N (Figure 11) suggests that the hysteresis decreases for both pre-crept microstructures. As noted earlier, this corresponds to a decrease in the frictional resistance to interfacial motion and a lower rate of dissipation of the stored elastic energy (Refs. 30, 31, and 32). However, the hysteresis is narrower for the specimen pre-crept at 473 K than for the one pre-crept at 300 K. Since M_s increases with increasing N while M_f is constant for both pre-crept specimens (Figure 11), the stored energy in the martensite is high and less heating is required to initiate the reverse martensite-to-austenite transformation (Refs. 30, 31, and 32).

There is now considerable microstructural evidence that thermal cycling conducted with and without an applied constant load results in a significant increase in the dislocation density with each thermal cycle (Refs. 5, 6, 10, 29, 32, 33, and 34). The measured dislocation densities increased from 10^{10} to 5×10^{14} m^{-2} after 100 thermal cycles under no external load conditions (Refs. 10 and 34). Several recent observations indicate that dislocation glide loops are emitted into the austenite in front of an advancing austenite-martensite interface during the forward transformation from austenite to martensite to accommodate the formation of the martensite (Refs. 6, 10, 11, 30, and 34). No doubt the generation of these dislocations can account for the observed irrecoverable strains (Figure 8). The presence of these dislocations results in a back stress on the austenite-martensite interface therefore requiring a larger driving force for martensitic transformation and a decrease in M_s with increasing N (Refs. 10 and 34). It has been suggested that the presence of retained martensite also contributes to the irrecoverable strain (Refs. 11 and 29) although retained martensite is not always observed (Ref. 7). In this case, the martensite is assumed to be stabilized by the dislocation structure so that M_s increases with increasing N (Ref. 29). Mechanical twins and pseudo-twins in the austenite have also been observed during thermomechanical cycling of NiTi (Ref. 4). Clearly, the plasticity of the austenite can be attributed to either the activation of at least five independent slip systems (Ref. 11) or a combination of deformation twins and dislocation slip to satisfy von Mises criteria (Ref. 27).

In view of the above discussion, the areas under the ε̇-T plots are measures of either the rates of increase in the stored elastic strain energy during the forward transformation (Figure 9(a) and (b)) or the dissipation of the stored elastic strain energy during the reverse transformation (Figure 9(c) and (d)). An examination of Figure 9(a) and (b) reveals that the ε̇–T plots are fairly similar irrespective of the initial pre-crept microstructure thereby suggesting similar amounts of stored elastic energy in both cases. Remarkably, the curves are well-defined and overlap each other after each cycle with the peak strain rate values occurring between 364 and 368 K suggesting that the transformation of the austenite to martensite is unaffected by any microstructural variation caused by the martensite to austenite transformation in the

previous reverse cycle. In contrast, the pre-crept microstructures have a significant effect on the dissipation of the stored elastic energy during the reverse transformation. The ε̇–T plots for the specimen pre-crept at 473 K are well-defined and overlap after the first thermal cycle and the martensite transforms to austenite over a broad temperature range (Figure 9(c)). The troughs for the curves, which occur between about 410 and 430 K, have a relatively broad spread of about 20 K. Assuming that the initial pre-crept microstructure consisted of a mixture of dislocations and deformation twins in the B2 austenite, coupled with the fact that thermal cycling of NiTi generates additional dislocations in the austenitic phase (Refs. 6, 10, 11, 30, and 34), the present observations suggest that the wide temperature range over which the reverse transformation occurs is influenced by the development of the internal stresses in the material. Therefore, it is reasonable to suggest that these local internal stresses oppose the progress of the austenite-martensite interfaces in the material during the reverse transformation so that the martensite transforms sluggishly to austenite. Under local stress conditions favorable to stabilizing the martensite, it is unlikely that martensite will transform to austenite so that it is retained at 473 K.

In comparison, the ε̇–T curves are well-separated for each cycle with relatively sharp troughs for the specimen pre-crept at 300 K, where the trough decreases from 477 K for cycle no. 1 to 456 K for cycle no. 3 (Figure 9(d)). Interestingly, the spread in the curves increases from the first to the third cycle before becoming approximately constant while the martensite starts transforming to austenite at lower and lower temperatures with each thermal cycle. Since the pre-crept microstructure is expected to consist predominantly of single variant martensitic twins with a few dislocations generated during isothermal primary creep, the differences in the characteristics of the curves for cycles nos. 1 and 2 are revealing. It should be noted that since dislocations are generated during the forward transformation (Refs. 5, 6, 10, 29, 30, 33, and 34), the microstructure of the specimen prior to cycle no. 2 is expected to consist of a significant number of dislocations. Thus, the observed broadening of the curves after cycle no. 1 can be attributed to a significant increase in the dislocation density and a corresponding increase in the internal stresses in the material similar to the case for the specimen pre-crept at 473 K. Thus, the observed differences in the nature of the plots shown in Figure 9(c) and (d) stem from the fact that the curves for the specimen pre-crept at 300 K are in the process of evolving towards those for the specimen pre-crept at 473 K. Eventually, it is expected that the curves for both specimens would be similar after a sufficiently large number of thermal cycles.

As noted earlier, the reverse transformation from martensite to austenite commences at lower and lower temperatures (Figure 9(c) and (d)) thereby resulting in a decrease in A_s with increasing N (Figure 11). The precise reason for this is unclear at this time but several possibilities exist. First, it is possible that some of the austenite fails to transform as thermal cycling progresses. However, it is important to note that retained austenite has not been observed in the alloy used in the present investigation although recent results on the short-term creep of a Ti-rich NiTi deformed at 773 K revealed the presence of retained austenite (Ref. 18). Second, the skewness in the curves towards the lower temperatures could be attributed to the transformation of favorably oriented martensitic twins to twins in the austenite during the reverse transformation. Ii et al. (Ref. 21) observed a direct correlation between the $\{20\overline{1}\}_{B19'}$ twins in the deformed martensite and the $\{114\}_{B2}$ twins in austenite during reverse transformation in in-situ microstructural experiments conducted on a Ti-50.6at.% Ni alloy. It is also worth noting that $\{114\}_{B2}$ deformation twins were observed in a NiTi alloy after thermal cycling under a constant load (Ref. 4). Third, an increase in M_s with increasing N (Figure 11) has been attributed to the stability of the martensite (Ref. 29), so that it is possible that the local stress fields around some martensitic plates prevent them from transforming back to austenite during the reverse transformation so that the volume fraction of the retained martensite increases with increasing N. In that case, the amount of martensite available for transformation back to austenite will correspondingly decrease so that A_f would decrease with increasing N. Clearly, further studies are needed to elucidate these issues.

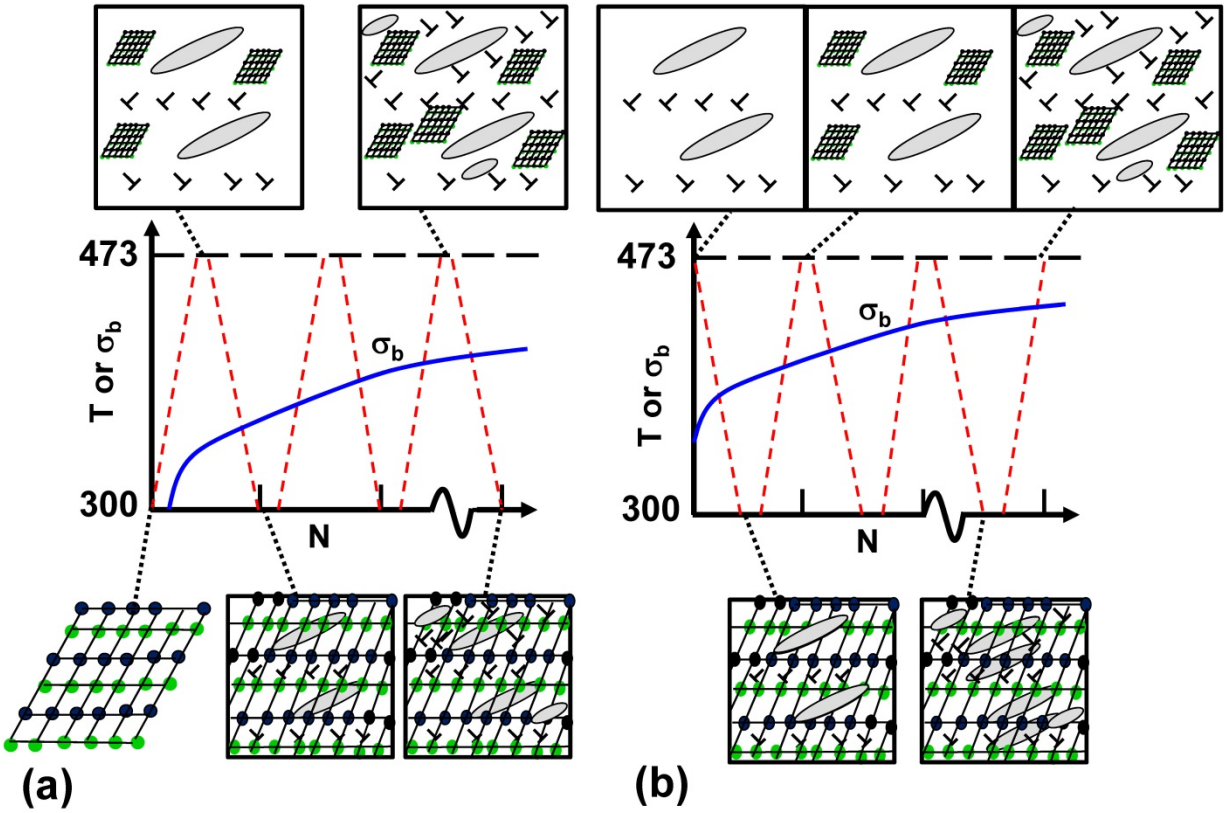

Figure 13.—Schematic showing the effect of thermal cycling on the evolution of the microstructure and back stresses, σ_b, for specimens pre-crept at: (a) 300 K and (b) 473 K. The austenite deforms by a combination of deformation twinning and dislocation slip, while the martensite deforms by detwinning. As the specimens are thermally cycled between 300 and 473 K, dislocations are generated in the austenite so that σ_b increases with increasing N until the microstructure stabilizes. The smooth curve represents the increase in σ_b with increasing N. Some of the martensite is retained at 473 K under the action of the local internal stresses.

Figure 13(a) and (b) are schematic representations showing the evolution of the microstructure during thermal cycling for the two specimens with different pre-crept microstructures. In Figure 13(a), the specimen with the detwinned martensitic pre-crept microstructure is heated to the austenitic region above A_f under an applied stress during the first half of the thermal cycle. The martensite transforms to austenite, where the deformation and transformation strains are accommodated by dislocation slip, and possibly deformation twinning, with a corresponding increase in the back stress, σ_b, in the specimen. It is expected that some of the martensite would be stabilized by local internal stresses, and therefore, these martensitic plates would not transform to austenite. Thus, the expected microstructure at 473 K in the austenite at the end of this half cycle consists of a combination of glide dislocations, deformation twins and untransformed martensitic plates. In the second half of the thermal cycle, the austenite transforms back to martensite but the deformation twins and dislocations remain in the matrix since there is no significant recovery at these temperatures. However, there is a distinct possibility that the $\{114\}_{B2}$ deformation twins in the austenite transform to $\{20\overline{1}\}_{B19'}$ martensitic twins (Ref. 21). In addition, based on experimental evidence (Refs. 6, 10, 11, 30, and 34), it is expected that the dislocation density would increase substantially to accommodate the transformation strain. On reverse transformation in the first half of the subsequent cycles, it is suggested that the $\{20\overline{1}\}_{B19'}$ martensitic twins nucleate the $\{114\}_{B2}$ deformation twins in the austenite so that these twins flip-flop every half thermal cycle. The back stress increases with increasing number of thermal cycles, so that the effective stress, $\sigma_{eff} = (\sigma - \sigma_b)$, decreases in the matrix thereby resulting in a corresponding nonlinear increase in ε_A and ε_M (Figure 5), and a

decrease in $(\Delta\varepsilon_{irr})_A$ and $(\Delta\varepsilon_{irr})_M$ with increasing N (Figure 8). Assuming a Taylor-type hardening mechanism (Ref. 35), the effective stress is dependent on the dislocation density, ρ_d, and deformation twin density, ρ_t,

$$\sigma_{eff} = (\sigma - \sigma_b) = \sigma_0 + \alpha M \mu_A b_A (\rho_d + \rho_t)^{-0.5} \quad (3)$$

where σ_0 is the lattice friction stress, M is the Taylor factor, α is a constant, μ_A is the shear modulus of the austenite and b_A is the Burgers vector for the austenite. Eventually, when N = n, the microstructure stabilizes (Figure 13(a)) so that A_s and A_f become independent of N.

The response of the specimen pre-crept at 473 K results in a larger value of σ_b prior to the start of the thermal cycle experiments owing to the presence of dislocations and deformation twins generated during isothermal primary creep (Figure 13(b)). Cooling down to 300 K in the first half of the thermal cycle results in the transformation of the austenite to martensite while retaining the deformation twins and dislocations present in the pre-crept microstructure. From the second half of the first thermal cycle and beyond, the microstructure and σ_b develop in a manner similar to that described above for the specimen pre-crept at 300 K (Figure 13(a)) except that the microstructure reaches a stable state at a lower value of N.

The observations reported in this paper have important implications for actuator design and bring into question the stability of binary NiTi alloys during thermal cycling. As noted in Part I (Ref. 1), the objective of this investigation was to understand the origin of the irrecoverable strain, which arises as near-stoichiometric NiTi is thermally cycled under a constant applied stress (Figure 1 to Figure 3). It was demonstrated in Part I that NiTi undergoes significant primary creep at 473 K when the applied stress exceeds 220 MPa; the alloy creeps at a much lower rate at 300 K for applied stresses greater than 200 MPa. However, as demonstrated in Part II, thermal cycling between 300 and 473 K under creep stresses identical to those used in the isothermal experiments results in a significant amount of thermal ratcheting to 15 to 20 percent. The fact that the creep strain was immeasurably small for hold times varying between 300 and 700 h at each temperature convincingly demonstrates that irrecoverable strain accumulation due to thermal cycling far exceeds that due to isothermal creep due to a significant increase in the dislocation density in the austenite (Refs. 5, 6, 10, 29, 30, 33, and 34).

Clearly, the magnitude of the irrecoverable strain is determined by the deformation of the austenitic phase. Thus, strengthening of the austenitic phase against dislocation slip is expected to improve the long term stability of the actuator and increase its life. Traditionally, this process has involved thermally cycling NiTi over a large number of cycles in an attempt to develop a stable microstructure through a process called “training” (Ref. 36). However, the problem with this approach is that a stable dislocation substructure is generally attained only after several hundred thermal cycles, which is not only expensive but it is also likely to reduce the work output of the actuator. As demonstrated in this investigation, the dislocation substructure tends to stabilize within a few thermal cycles if the alloy is initially pre-crept in the austenitic phase region. Nevertheless, it must be recognized that the stability of the dislocation microstructure is limited to the stress and temperature conditions under which it was generated and changes in the operating conditions of the actuator can destabilize the dislocation microstructure.

5.0 Summary and Conclusions

This paper is the first report on the effect of prior low temperature creep on the thermal cycling behavior of NiTi. Specimens isothermally pre-crept at 300 and 473 K for several thousand hours were thermally cycled between 300 or 373 and 473 K under applied stresses of either 250 or 350 MPa. The present observations revealed that the total strain significantly ratchets up with each thermal cycle irrespective of the initial creep microstructure with the strain contribution from isothermal creep during hold times at each temperature being negligible. It is demonstrated that the strains in the austenite and martensite decrease non-linearly with increasing number of thermal cycles thereby suggesting a hardening of the alloy due to the development of back stresses as dislocations are generated in the material during each thermal cycle. The differential irrecoverable strain, $\Delta\varepsilon_{irr}$, varies with N as $\Delta\varepsilon_{irr} = 4.3\ N^{-0.5}$ similar to

the Manson-Coffin relationship observed in low cycle and thermal fatigue. The magnitudes of A_s and A_f temperatures were observed to be sensitive to the isothermal pre-crept microstructure with these transformation temperatures being higher when the specimen was pre-crept in the martensitic phase field at 300 K compared to that pre-crept in the austenitic phase field at 473 K. Both of these transformation temperatures decrease with increasing N when the pre-crept microstructure consists of detwinned martensite. Similarly, A_s also decreased with increasing N, but A_f was constant when the pre-crept austenitic microstructure likely consisted of dislocations and deformation twins. A phenomenological model is proposed to rationalize the observations reported in this paper, which suggests that the back stress increases with increasing N due to dislocation generation in the austenite.

References

1. S. V. Raj, R. D. Noebe, submitted to Mater. Sci. A.
2. J. Ma, I. Karaman, R. D. Noebe, Intern. Mater. Rev. 55 (2010) 257-315.
3. T. Saburi, in: K. Otsuka, C.M. Wayman (Eds.), Shape Memory Materials, Cambridge University Press, Cambridge, U.K., 1998, pp. 44-96.
4. E. Goo, T. Duerig, K. Melton, R. Sinclair, Acta Metall. 33 (1985) 1725-1733.
5. S. Miyazki, Y. Igo, K. Otsuka, Acta Metall. 34 (1986) 2045-2051.
6. T. Simon, A. Kröger, C. Somsen, A. Dlouhy, G. Eggler, Acta Material., 58 (2010) 1850-1860.
7. R. Delville, B. Malard, J. Pilch, P. Sittner, D. Schryvers, Intern. J. Plastic. 27 (2011) 282-297.
8. S. Padula, S. Qiu, D. Gaydosh, R. Noebe, G. Bigelow, A. Garg and R. Vaidyanathan, Metall. Mater. Trans. 43A (2012) 4610-4621.
9. S. Belyaev, N. Resnina, A. Sibirev, J. Alloy Comp. 542 (2012) 37-42, http://dx.doi.org/10.1016/j.jallcom.2012.07.082.
10. A. R. Pelton, G. H. Huang, P. Moine, R. Sinclair, Mater. Sci. Eng. A 532 (2012) 130-138.
11. T. Ezaz, J. Wang, H. Sehitoglu, H. J. Maier, Acta Mater. 61 (2013) 67-78.
12. A. K. Mukherjee, J. Appl. Phys. 19 (1968) 2201-2204.
13. H. Kato, T. Yamamoto, S. Hashimoto, S. Miura, Mater. Trans. JIM 40 (1999) 343-350.
14. E. Kobus, K. Neuking, G. Eggler, I. Wittkamp, Prakt. Metallogr. 39 (2002**)** 177-186.
15. G. Eggeler, J. Khalil-Allafi, K. Neuking, A. Dlouhý, Z. Metallkd. 93 (2002) 654-660.
16. C. Lexcelent, P. Robinet, J. Bernardini, D. L. Beke, P. Olier, Materialwiss. Werkstofftech, 36 (2005) 509-512.
17. S. M. Oppenheimer, A. R Yung, D. C. Dunand, Scripta Mater. 57 (2007) 377-380.
18. A. Ahadi, E. Rezaei, J. Mater. Eng. Perform. 21 (2012) 1806-1812.
19. K. Otsuka, X. Ren, Intermetall. 7 (1999) 511-528.
20. H. Sehitoglu, R. Hamilton, D. Canadinc, X. Y. Zhang, K. Gall, I. Karaman, Y. Chumlyakov, H. J. Maier, Metall. Mater. Trans. 34A (2003) 5-13.
21. S. Ii, K. Yamauchi, Y. Maruhashi, M. Nishida, Scripta Mater. 49 (2003) 723-727.
22. Y. Liu, Z. Xie, in: P. L. Reece (Ed.), Progress in Smart Materials and Structures, Nova Science Publishers, Inc., Hauppauge, NY, 2007, pp. 29-65.
23. J. X. Zhang, M. Sato, A. Ishida, Acta Mater. 54 (2006) 1185-1198.
24. T. Ezaz, Ph.D. Thesis, University of Illinois, Urbana-Champaign, IL, 2011.
25. T. Ezaz, H. Sehitoglu, Appl. Phys. Lett. 98 (2011) 241906.
26. T. Ezaz, H. Sehitoglu, W. Abuzaid, H. J. Maier, Mater. Sci, Eng. A 585 (2012) 422-430.
27. M. A. Meyers, K. K. Chawla, Mechanical Metallurgy: Principles and Applications, Prentice-Hall, NJ, 1984, p. 697.
28. K. N. Melton, O. Mercer, Acta Metall. 27 (1979) 137-144.
29. CH. Grossman, J. Frenzel, V. Sampath, T. Depka, G. Eggeler, Metall. Mater. Trans. 40A (2009) 2530-2544.
30. L. Delaey, J. Ortin, J. Van Humbeeck, Proc. in Phase Transformation 87, The Institute of Metals, London, U.K., 1988, pp. 60-66.

31. J. Van Humbeeck, E. Aeronoudt, L. Delaey, Lu Li, H. Verguts, J. Ortin, Revue Phys. Appl., 23 (1988) 595-601.
32. R. F. Hamilton, H. Sehitoglu, Y. Chumlyakov, H. J. Maier, Acta Mater. 52 (2004) 3383-3402.
33. T. Nishura, M. Nishida, Mater. Trans. 50 (2009) 1219-1224.
34. A. R. Pelton, J. Mater. Eng. Perform. 20 (2011) 613-617.
35. L. Zhu, H. Ruan, X. Li, M. Dao, H. Gao, Jian Lu, Acta Mater. 59 (2011) 5544–5557.
36. J. Van Humbeeck, R. Stalmans, in: K. Otsuka and C.M. Wayman (Eds.) Shape Memory Materials, Cambridge University Press, Cambridge, U.K., 1998, pp. 149-183.

REPORT DOCUMENTATION PAGE	Form Approved OMB No. 0704-0188

1. REPORT DATE *(DD-MM-YYYY)*	2. REPORT TYPE	3. DATES COVERED *(From - To)*
01-06-2013	Technical Memorandum	

4. TITLE AND SUBTITLE
Low Temperature Creep of Hot-Extruded Near-Stoichiometric NiTi Shape Memory Alloy
Part II: Effect of Thermal Cycling

5a. CONTRACT NUMBER

5b. GRANT NUMBER

5c. PROGRAM ELEMENT NUMBER

6. AUTHOR(S)
Raj, S., V.; Noebe, R., D.

5d. PROJECT NUMBER

5e. TASK NUMBER

5f. WORK UNIT NUMBER
WBS 561681.02.08.47.05.04

7. PERFORMING ORGANIZATION NAME(S) AND ADDRESS(ES)
National Aeronautics and Space Administration
John H. Glenn Research Center at Lewis Field
Cleveland, Ohio 44135-3191

8. PERFORMING ORGANIZATION REPORT NUMBER
E-18699-2

9. SPONSORING/MONITORING AGENCY NAME(S) AND ADDRESS(ES)
National Aeronautics and Space Administration
Washington, DC 20546-0001

10. SPONSORING/MONITOR'S ACRONYM(S)
NASA

11. SPONSORING/MONITORING REPORT NUMBER
NASA/TM-2013-217888-PART2

12. DISTRIBUTION/AVAILABILITY STATEMENT
Unclassified-Unlimited
Subject Category: 26
Available electronically at http://www.sti.nasa.gov
This publication is available from the NASA Center for AeroSpace Information, 443-757-5802

13. SUPPLEMENTARY NOTES
Submitted to Materials Science & Engineering A, Elsevier.

14. ABSTRACT
This paper is the first report on the effect prior low temperature creep on the thermal cycling behavior of NiTi. The isothermal low temperature creep behavior of near-stoichiometric NiTi between 300 and 473 K was discussed in Part I. The effect of temperature cycling on its creep behavior is reported in the present paper (Part II). Temperature cycling tests were conducted between either 300 or 373 K and 473 K under a constant applied stress of either 250 or 350 MPa with hold times lasting at each temperature varying between 300 and 700 h. Each specimen was pre-crept either at 300 or at 473 K for several months under an identical applied stress as that used in the subsequent thermal cycling tests. Irrespective of the initial pre-crept microstructures, the specimens exhibited a considerable increase in strain with each thermal cycle so that the total strain continued to build-up to 15 to 20 percent after only 5 cycles. Creep strains were immeasurably small during the hold periods. It is demonstrated that the strains in the austenite and martensite are linearly correlated. Interestingly, the differential irrecoverable strain, $\Delta\varepsilon_{irr}$, in the material measured in either phase decreases with increasing number of cycles, N, as $\Delta\varepsilon_{irr} = 4.3(N)^{-0.5}$ similar to the well-known Manson-Coffin relation in low cycle fatigue. Both phases are shown to undergo strain hardening due to the development of residual stresses. Plots of true creep rate against absolute temperature showed distinct peaks and valleys during the cool-down and heat-up portions of the thermal cycles, respectively. Transformation temperatures determined from the creep data revealed that the austenitic start and finish temperatures were more sensitive to the pre-crept martensitic phase than to the pre-crept austenitic phase. The results are discussed in terms of a phenomenological model, where it is suggested that thermal cycling between the austenitic and martensitic phase temperatures or vice versa results in the deformation of the austenite and a corresponding development of a back stress due to a significant increase in the dislocation density during thermal cycling.

15. SUBJECT TERMS
Low temperature creep; NiTi; Shape memory alloys; Thermo-mechanical cycling

16. SECURITY CLASSIFICATION OF:			17. LIMITATION OF ABSTRACT	18. NUMBER OF PAGES	19a. NAME OF RESPONSIBLE PERSON
a. REPORT	b. ABSTRACT	c. THIS PAGE			STI Help Desk (email:help@sti.nasa.gov)
U	U	U	UU	26	19b. TELEPHONE NUMBER *(include area code)* 443-757-5802